

Refinement of Modeling Techniques for the Structural Evaluation of Hanford Single-Shell Nuclear Waste Storage Tanks – 12288

Naveen K. Karri, Michael W. Rinker, Kenneth I. Johnson, Satish K. Bapanapalli
Pacific Northwest National Laboratory, Richland, WA 99352

ABSTRACT

The single-shell tanks at the Hanford Site (in Washington State, USA) were constructed between 1943 and 1964 and are well beyond their estimated 25 year design life. This article discusses the structural analysis approach and modeling challenges encountered during the ongoing analysis of record for evaluating the structural integrity of the single-shell tanks. There are several geometrical and material nonlinearities and uncertainties to be dealt with while performing the modern finite element analysis of these tanks. The analysis takes into account the temperature history of the tanks and allowable mechanical operating loads for proper estimation of creep strains and thermal degradation of material properties. The loads prescribed in the analysis of record models also include anticipated loads that may occur during waste retrieval and closure. Due to uncertainty in a number of modeling details, sensitivity studies were conducted to address questions related to boundary conditions that realistically or conservatively represent the influence of surrounding tanks in a tank farm, the influence of backfill excavation slope, the extent of backfill and the total extent of undisturbed soil surrounding the backfill. Because of the limited availability of data on the thermal and operating history for many of the individual tanks, some of the data was assumed or interpolated. However, the models developed for the analysis of record represent the bounding scenarios and include the loading conditions that the tanks were subjected to or anticipated. The modeling refinement techniques followed in the analysis of record resulted in conservative estimates for force and moment demands at various sections in the concrete tanks. This article discusses the modeling aspects related to Type-II and Type-III single-shell tanks. The modeling techniques, methodology and evaluation criteria developed for evaluating the structural integrity of single-shell tanks at Hanford are in general applicable to other similar tanks or underground concrete storage structures.

INTRODUCTION

The Hanford site in Washington State contains 177 underground concrete tanks used for the storage of nuclear waste generated since plutonium production began during the World War II era. Of the total, 149 are the first generation single shell tanks. All of the single-shell tanks are well beyond their estimated 25 year design life and some of them found to have leaked (or are categorized as assumed leakers) The single-shell tanks have been decommissioned (they cannot receive any new waste) and interim stabilized (pumpable liquids have been removed) by transferring the liquid waste into the newer constructed double shell tanks. Although the single-shell tanks currently don't hold any free liquids they still contain some waste in the form of salt-cake and sludge which needs to be cleaned before their permanent closure. Understanding the structural integrity of these single-shell tanks is necessary not only to carry out the waste retrieval and cleaning operations but also for their safe closure.

Since the existing structural analysis documents on single-shell tanks are nearly two decades old and some of them being tank specific, the U.S. Department of Energy (DOE) Office of River Protection (ORP) has recently determined the need to perform a modern finite element analysis of these single-shell tanks to understand their current structural integrity. The primary objective

of the single-shell tank analysis of record project is to perform a modern and comprehensive structural analysis for the single-shell tanks in order to understand the existing single-shell tank structural integrity as a result of past usage and natural hazard phenomena as well as their future integrity under anticipated loads during waste retrieval and closure or under a seismic event.

Based on the capacity to hold waste, single-shell tanks are classified into 4 types as shown in Table 1. The design configuration for each of the tank types is illustrated in Figure 1. Out of total 149 single-shell tanks, nearly 73% (108 tanks) are either Type-II or Type-III tanks and hence their analysis was carried out in the first phase of the analysis of record project. The second phase of the analysis of record project concentrates on Type-I and Type-IV single-shell tanks. However, the modeling challenges and resolutions presented in this article are also applicable to Type-I and Type-IV tanks.

Table I. Classification of Single-Shell Tanks

Type	Farms	Tanks Include
I	241-C, 241-T, 241-B, 241-U	200-series, 20-foot Φ , 50k gal
II	241-C, 241-T, 241-B, 241-U, 241-BX	100-series, 75-foot Φ , 500k gal
III	241-S, 241-BY, 241-TX, 241-TY	100-series, 75-foot Φ , 750k gal
IVA	241-SX	100-series, 75-foot Φ , million gal
IVB	241-A	100-series, 75-foot Φ , million gal
VC	241-AX	100-series, 75-foot Φ , million gal

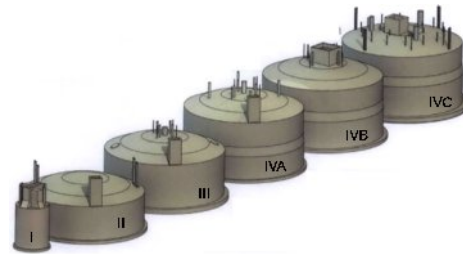


Fig 1. Single-Shell Tanks Configuration

The details of modeling techniques and the analysis approach taken during the finite element modeling of Type II and Type III single-shell tanks are presented in the following sections. The single-shell tank structural integrity was evaluated by performing a thermal and operating loads analysis, as well as seismic analyses. These analyses include loading conditions described in the evaluation criteria report by Johnson et al [1]. The loads considered in the Type II and the Type III detailed finite element models include dead, live, and seismic loads. The thermal and operating load analysis and seismic models were analyzed independently, and then selected thermal and operating load analysis and seismic results were combined to obtain demand-to-capacity (D/C) ratios in accordance with the American Concrete Institute code, ACI 349-06 [2]. The resulting demands from the tank finite element models were compared to the corresponding section capacities at various locations in the tanks to determine the structural integrity. This article presents two key modeling challenges encountered during thermal and operating load analysis and the sensitivity studies conducted to overcome those challenges. The details of seismic modeling could be found in Abatt et al. [3] and the combination of thermal and operating load analysis and seismic results for integrity evaluation could be found in Pilli et al. [4] articles.

TYPE II AND TYPE III TANK MODELS

Tank Geometries

The Type II and Type-III tanks are underground, reinforced-concrete tanks with a 75-foot internal diameter and capacities of 530,000-gallon and 758,000-gallon respectively. The Type-II tanks were constructed between 1943 and 1948 and the Type-III tanks were constructed between 1947 and 1952. Both types of tanks have similar dome geometries with minor

changes in rebar schedule. There are some differences in the Type-II and Type-III tank walls and slabs. While the Type-II tanks have 12-inch thick walls with 6-inch uniform thick slab, the Type-III tanks have 15-inch thick walls with a slab whose thickness varies from 6-inch at the centerline to 18-inch near the footing. The steel liner in either type of tanks is not attached to the cylindrical wall and does not contribute significantly to the structural integrity of the reinforced concrete tank shell. The purpose of the liner is only to serve as a leak barrier and hence it is not included in the structural analysis.

Model Development

The Type II and Type III tank finite element models are very similar in their features and material models, except for the differences in the tank geometries. ANSYS® [7] Version 12.0 was used in all the thermal and operating load analysis analyses of the Type II and Type-III single-shell tanks. The finite element models are 3-D slice models obtained by rotating the 2-D section geometry through 2-degrees around the tank central axis. The rotation angle was chosen to obtain elements of good aspect ratios in the finite element model. Although the thermal and operating load analysis loads are axisymmetric, 3-D slice models were required because the concrete elements in ANSYS® are only 3-D. The Type-II tanks were modeled with a soil overburden of 10 ft and the Type III tanks were modeled with 11 ft overburden. The sub-grade undisturbed soil depth is specified at 168 ft below the foundation in the finite element models. Following the double shell tanks thermal and operating load analysis approach [5], the radial extent of the soil (lateral soil dimension) was modeled to a radius of 240 ft. The compacted backfill excavation slope boundary that distinguishes backfill soil from undisturbed soil was not modeled in the thermal and operating load analysis and instead the backfill soil was modeled throughout the lateral extent. The rationale for using backfill soil for all soil above the tank foundation level is presented in the later sections of this article. The Type-II and Type-III finite element models include six and seven layers of backfill soil respectively above the tank foundation level. In both models, the undisturbed soil beneath the tanks is modeled to a depth of 168-ft with eight stratigraphic soil layers. The material properties for the concrete and soil are summarized in the single-shell tank Evaluation Criteria report [1].

The ANSYS® SOLID65 [7] (3-D Reinforced Concrete Solid) elements with the ability to simulate cracking (in tension), crushing (in compression), and creep are used to represent concrete regions with and without reinforcement (rebars). The reinforcement model in the SOLID65 elements is a smeared model and requires specifying the amount of steel in each element as a volume fraction of the total element volume. The reinforcement properties are input as real constants which include the material number, the volume ratio, and the orientation angles. The soil surrounding the tank is modeled with SOLID185 [7] elements, with the Extended Drucker-Prager material model. The nonlinear contacts at the concrete and the soil interface use TARGE170 [7] and CONTA173 [7] elements.

Figure 2 illustrates some of the details of the single-shell tank analysis of record finite element models. In this figure the top left quadrant (a) present the full model and geometrical details of the tank and the extent of surrounding soil till the boundaries considered for analysis. The top right quadrant (b) present the magnified view of various important sections of the concrete shell along with the section names referred from here after in the article. The bottom left quadrant (c) illustrates the magnified view of haunch region shown in (b) along with the details of rebar modeled in the haunch. The bottom right quadrant (d) illustrates the magnified view of knuckle and footing regions of the tank along with details of rebar modeled in those locations.

While calculating the volume fraction of steel for real constants careful consideration was given to match the total amount of steel in the in-plane (meridional) and the out-of-plane (hoop) directions. The locations of the reinforcement layers (represented as 1" thick elements) were also accurately defined in the cross-section thickness to accurately model the bending resistance of the reinforcing bars.

The ANSYS® concrete model has no provision for simulating the post-cracking tension stiffening behavior of reinforced concrete. The reinforced concrete elements instantly lose their total stiffness upon cracking resulting in numerical instability leading to solution convergence difficulties. In order to overcome the convergence issues, the unreinforced concrete elements were also given negligible non-zero reinforcement by assigning a reinforcement volume fraction of 0.01% of the element volume. The use of this augmented stiffness greatly enhanced the numerical stability of the model and it was demonstrated to have no significant impact on the resulting force, moment, stress, or strain calculations.

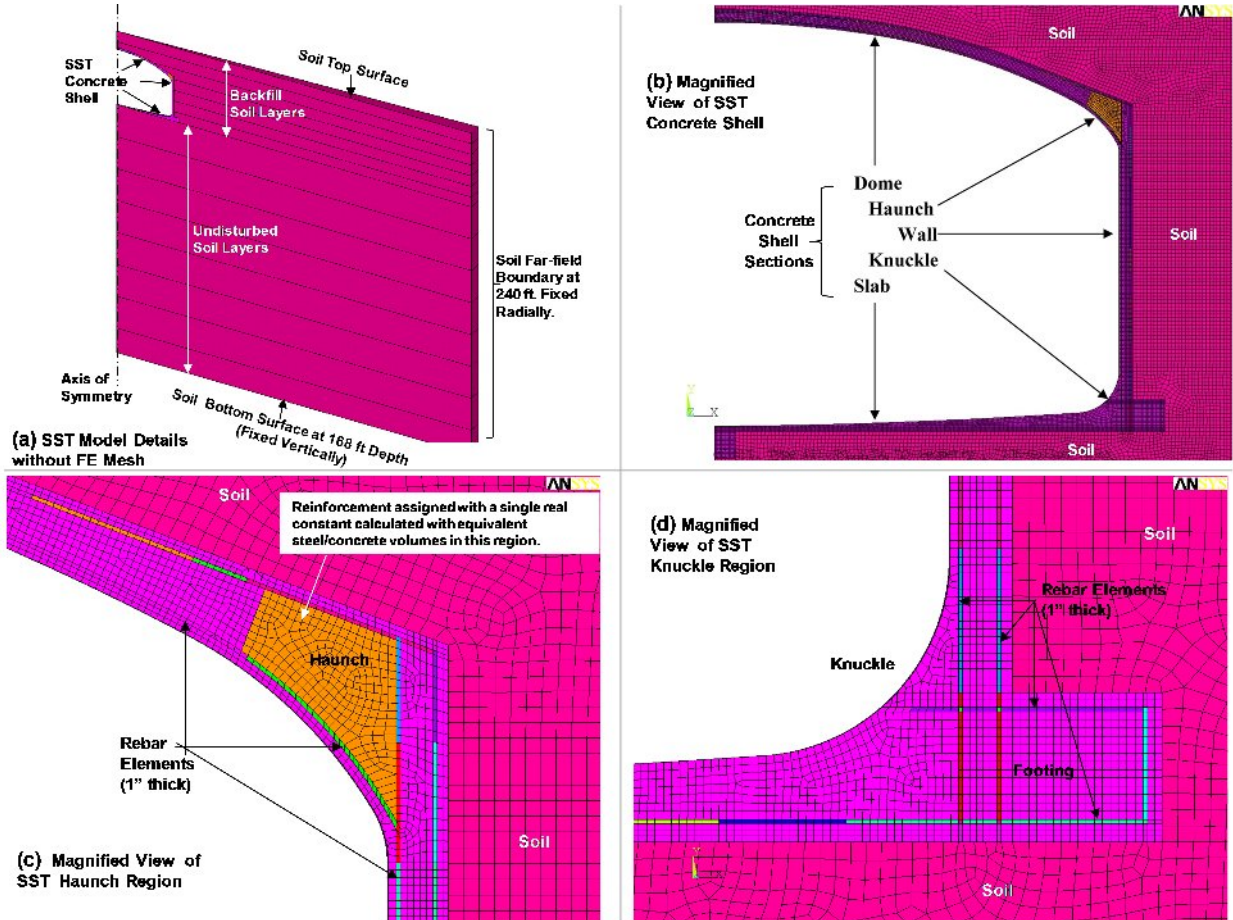


Fig 2. Finite Element model details of Type-III Single-Shell tank (a) Top-Left: Full model (b) Top-Right: Details of concrete shell (c) Bottom-Left: Close-up of Haunch region (d) Bottom-Right: Close-up of Knuckle/Footing region

Material Models

The ANSYS® concrete material model that allows for cracking and crushing, as well as variable shear transfer for open/closed cracks, is used for the SOLID65 elements. In addition, a custom creep model for concrete as described by the time-hardening creep Equation (1) was also input to account for thermally induced creep throughout the tank thermal history. The deduction of constants in the creep equation was based on the concrete literature data available for Hanford concrete. The details of this literature along with the procedure for calculating creep constants are presented in Johnson et al. [1].

$$\dot{\epsilon}_{cr} = C_1 \sigma^{C_2} t^{C_3} e^{-C_4/T} \quad (1)$$

Where C_1 , C_2 , C_3 , C_4 are creep constants, “t” represents time and “T”, temperature.

The structural analysis report of the C-106 single-shell tank [6] is the source of the temperature-dependent stress-strain curves that were used for the rebar in the single-shell tank analyses. Figure 4 shows the stress strain curves for Grade 40 rebar at temperatures ranging up to 400°F.

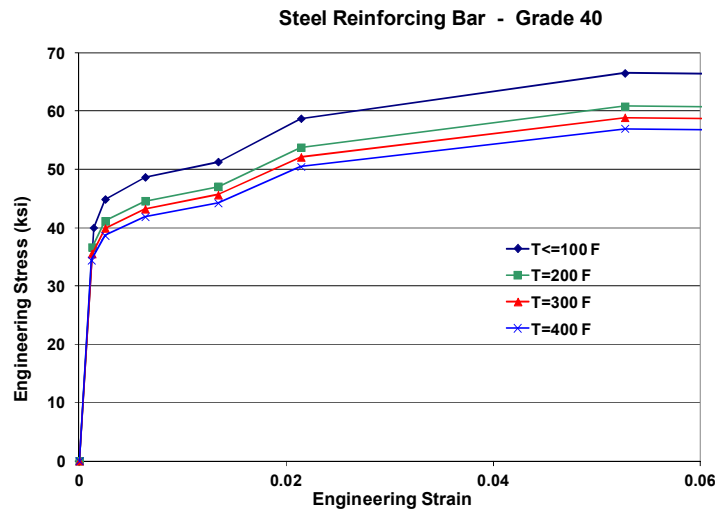


Fig 3. Stress-Strain Curves used for Grade 40 Steel Reinforcing Bar

The soil elements use the Extended Drucker-Prager [7] constitutive model, which has an internal friction angle, cohesion, and dilatancy angle as material properties. A small positive value of cohesion was used to represent the Hanford cohesionless soils. The ANSYS® Extended Drucker-Prager material model also requires specification of yield surface and flow potentials. A linear yield function and linear flow potential function were prescribed for the soil Extended Drucker-Prager material behavior in these analyses models. The soil-structure interaction between the tank and the surrounding soil was modeled using surface-to-surface contact elements with the sliding friction coefficient values prescribed in Table II. At the beginning of the analyses the side walls and other vertical surfaces in contact with soil were assigned a very small friction coefficient value of 0.05 to avoid any drag down loads on the tank

wall as gravity compresses the soil. After applying gravity, the friction coefficient was increased to a realistic value of 0.5.

Table II. Coefficients of Friction Used in the single-shell tank Structural Analysis

Material Interface	Location in Tank	Coefficient of Friction
Soil-to-Concrete	Dome	0.3
	Side Walls (before Gravity)	0.05
	Side Walls (after Gravity)	0.5
	Base Mat	0.6

Loads and Boundary Conditions

The Type II and Type III thermal and operating load analysis models consider the following mechanical live and dead loads.

- Soil load (an overburden of 10 ft for Type-II and 11ft for Type-III @ 125 lb/ft³ density) and self-weight of the tank applied by gravity.
- Historical hydrostatic loads due to waste applied as pressure loads on the inner surface of the tank
- 40 lb/ft² uniform surface live load to account for snow, ash fall applied as pressure on the top surface of the soil
- 200,000-lb concentrated live load distributed over 20-ft-diameter circular area concentric with the tank applied as a pressure load at the top surface of the soil to account for crane loads or other temporary equipment.

The mechanical loads were applied in the model in three load steps; the first load step solves for the gravity (self weight and soil overburden), the second load step solves for the initial hydrostatic waste load, and the third load step solves the additional surface live loads. The transient thermal loads along with variable hydrostatic waste loads were applied to the model in several load steps beginning from load step four.

In the finite element models, the base of the soil column is constrained in the vertical direction by specifying a boundary condition of no vertical translation. Similarly, the sides of the soil column are confined radially with a boundary condition of no radial translation. The front and back faces of the slice are given symmetric boundary conditions. These boundary conditions are applicable to structural models with mechanical as well as thermal loads.

The thermal loads on the tank (temperature profiles) at any point of time during the tank's operating history are dependent on the waste temperature and level in the tank. These thermal loads were determined from 2-D axisymmetric, transient thermal models that were developed to bound the operational histories of the Type II and Type III tanks, respectively. The details of these transient thermal analysis models are described in the next section. The thermal distributions obtained from the 2-D thermal models were imposed on the 3-D structural model simulating the historical thermal loads on the tanks. The thermal and operating load analysis models consider the irreversible thermal degradation of concrete strength and stiffness during the tank's service history. The property degradation is incorporated in the model by locking in the degraded material properties when the tank sections reach the peak temperatures in time. This prevents the concrete properties from "healing" when the tank cools.

Temperature Histories and Thermal Models

The temperature and waste height profiles shown in Figure 4 and Figure 5 were used for the detailed analysis of the Type-II and the Type-III tanks respectively. These profiles were deduced from the available single-shell tank temperature data from various databases and the literature. While the Type II tanks temperature profiles at various locations in the tank were obtained from the C-106 single-shell tank analysis [6] the Type-III tank bounding profiles were based on available data for S-101 and S-104 tanks. The details behind the development of thermal profiles and the 2-D axisymmetric transient thermal models are available in the Type-II analysis of record [8] and Type-III analysis of record [9] reports.

One addition in the 2-D axisymmetric thermal models was the waste surface as shown in Figure 6. The waste surface was added to simulate radiation and lumped convection heat transfer from the waste surface to the tank dome and walls. Radiation surfaces have been identified in Figure 6 with the aid of red and blue arrows. ANSYS® calculates the radiation view factors for all element surfaces based on the axisymmetric model.

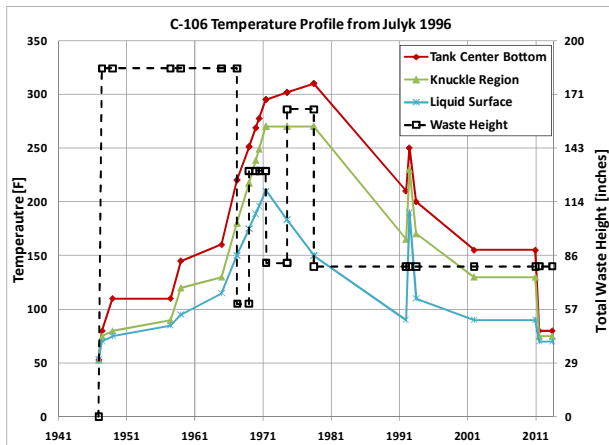


Fig 4. Temperature Profiles (°F) at Type II Tank Bottom, Knuckle and Liquid Surface along with waste height history plot (inches) showed as dashed line.

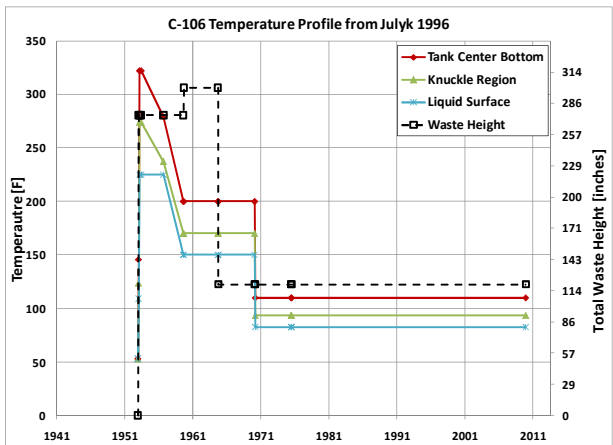


Fig 5. Temperature Profiles (°F) at Type III Tank Bottom, Knuckle and Liquid Surface along with waste height history plot (inches) showed as dashed line.

Loads on the thermal model were specified in the form of temperatures on the inner surface of the tank. Waste temperatures were imposed in the model by assigning the waste temperature values to the nodes on the inner surface of the tank that are located at or below the waste height. Waste temperature was assumed to vary linearly from the tank bottom temperature to the knuckle region (Figure 6). Similarly, the temperature was assumed to vary linearly from the knuckle to the liquid surface temperature. Temperature variations imposed on the inner surface of the tank slab and tank wall are schematically illustrated with black arrows representing the gradient in Figure 6. The bottom surface of the soil at 168 ft depth was assigned an isothermal boundary condition with a temperature value of 55°F representing the water table. A convective boundary condition with an average ambient air temperature of 53°F and a heat transfer coefficient of 2 Btu/h-ft²-°F was specified at the top surface of the soil. The right end (distant boundary) of the soil was prescribed with an adiabatic boundary condition.

The waste height profiles in Figure 4 and Figure 5 show different waste heights throughout the history of tanks operation. In order to account for the variation in waste height, the thermal analysis was split into several different sub-analyses every time the height changes. The nodal temperatures obtained from the thermal analysis were imposed as body forces on the nodes of the two-degree thermal and operating load analysis slice models. Figure 7 shows typical temperature distribution contours in the full thermal model, including the soil.

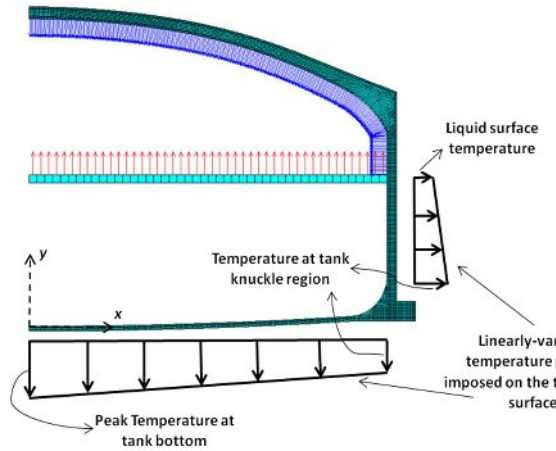


Fig 6. The 2-D Thermal Model Showing the Mesh in the Tank Structure and the Mesh in the Waste Surface.

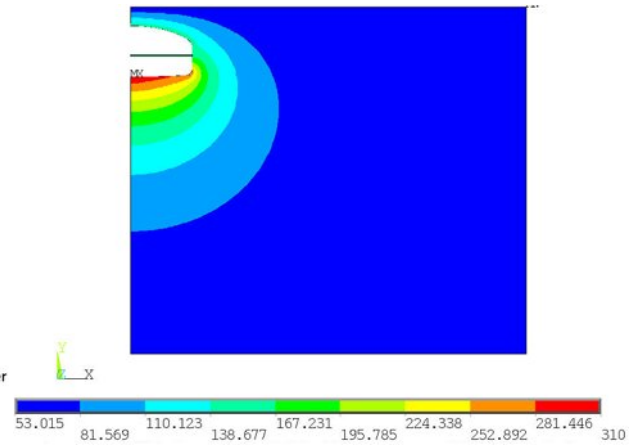


Fig 7. Temperature Distribution in single-shell tank and Surrounding Soil at Peak Temperature

Sensitivity Studies

Two of the main challenges encountered during the thermal and operating load analysis of the single-shell tanks are related to the far-field soil boundary (modeling of interaction effects of the surrounding tanks in a tank farm), and the extent of backfill soil in the models. Figure 8(a) shows the typical layout plan of Type II tanks with a 12 tank array. As shown in this figure, the tank-to-tank distance in the Type-II and the Type-III tank farms is about 100 ft. Figure 8(b) illustrates the soil configuration adjacent to the outermost tanks in a tank farm. According to these specification drawings, the excavation boundary with 1.5:1 run-to-raise ratio starts at nearly 10 ft from the outer face of the tanks foundation ring. Also, after the construction, the excavated soil is replaced with backfill soil that has higher density and a lower modulus than the undisturbed surrounding soil. Since the single-shell tank finite element models are axisymmetric models, the modeling of the excavation boundary and the extent of back fill are not straight forward.

The challenge lies in the fact that very few (2) of the tanks in a tank farm are completely surrounded by other tanks where the far-field rigid boundary must be at the location where the adjacent tank exists, i.e. 62 ft from the center of any tank. However, most of the tanks are not completely surrounded and there exists an infinite far-field soil on one (outer middle tanks) or two (corner tanks) sides. Another challenge is in modeling the backfill soil. If one of the middle tanks is considered, the backfill soil surrounding the tanks extend to more than 1.5 times the tank diameter (75 ft) where as the outer tanks have the excavation boundary on one or two of its sides and the back fill soil end at these boundaries. The asymmetric boundary conditions described so far are too complex and computationally intensive to model realistically. Hence, sensitivity studies were conducted to address the issues of (a) the usage of backfill instead of undisturbed soil surrounding the tanks and (b) the radial extent of soil required in the thermal

and operating load analysis models. Since it is not possible to model the exact backfill configuration, the rationale is to choose a simpler backfill configuration that bounds the other cases. Based on the results from these sensitivity studies, the modeling methods that yield conservative results were followed in the Type-II and Type-III tanks analysis of record.

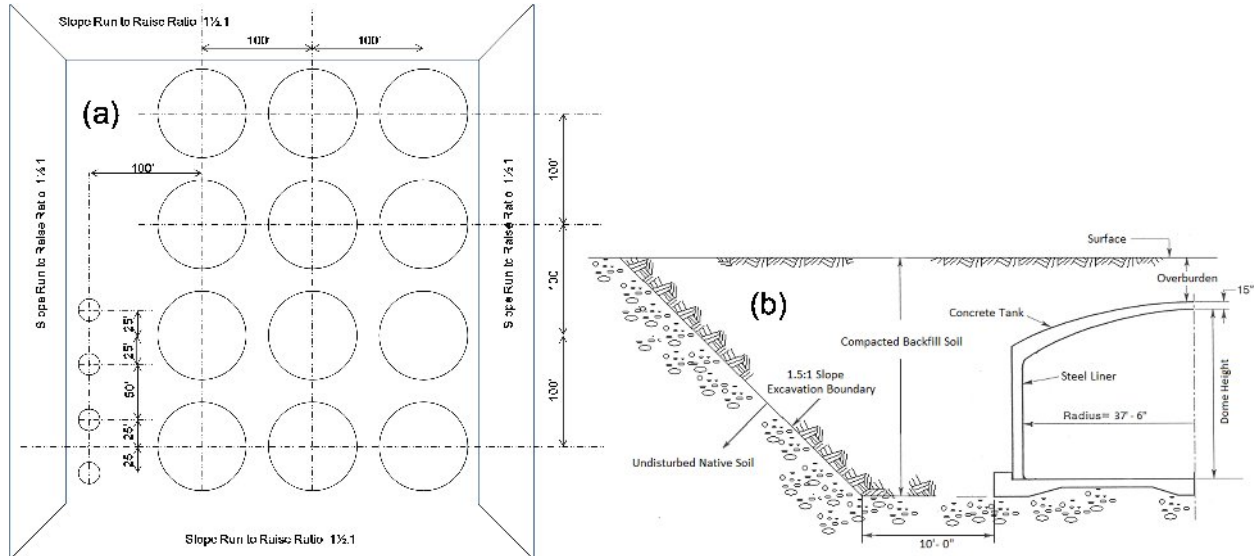


Fig 8. (a) Typical Type-II Tank Farm Layout (b) Typical Soil Configuration Adjacent to Type-II and Type III Tanks

The single-shell tank finite element models with materials properties discussed in previous sections were used in the sensitivity studies as well. The models used in the analysis of record as well as for the sensitivity studies use near zero (10 psi) tensile strength concrete due to the likelihood of widespread cracking during curing and thermal cycling of the concrete tanks. This is a common practice followed in the analysis of concrete structures [10, 11], and it is also consistent with the ACI evaluations that do not allow taking credit for the tensile capacity of concrete. In the following discussions, the term “near-zero” represent the models run with 10 psi concrete strength throughout the analysis. This small value of 10 psi is taken instead of zero to assure convergence in the simulations.

Figure 9 illustrates some of the features of the “baseline” single-shell tank finite element model for the sensitivity studies. This again is a 2-degree slice model with 240-ft radial soil extent. The excavation boundary starts at 10 ft from the outer radius of the foundation slab (footing) and has a run-to-raise ratio of 1.5:1. There are six layers of backfill and six layers of surrounding undisturbed soil. The soil beneath the tank was modeled with eight layers. The baseline model has backfill up to the excavation boundary with native soil extending to the 240 ft boundary. The structural and thermal boundary conditions discussed in previous sections are applied to the model. However, a simplified thermal history profile as shown in Figure 10 is used in these sensitivity studies.

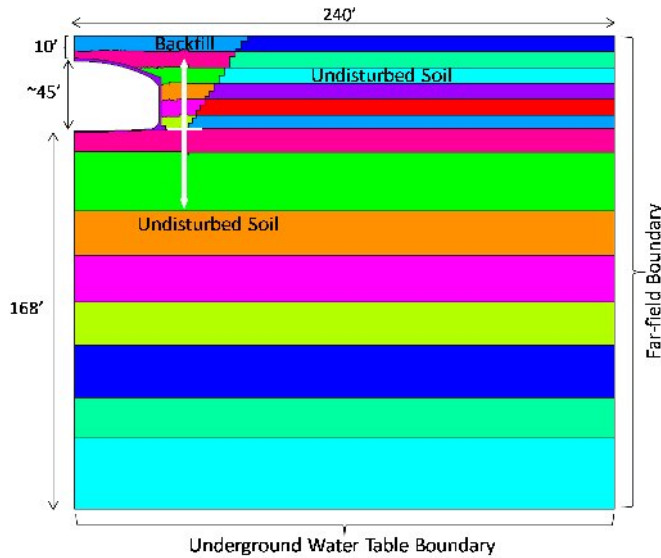


Fig 9. Baseline Single-Shell Tank finite element Model for Sensitivity Studies

The sensitivity studies (using Type-II analysis of record models) were evaluated at the 3 points shown on the temperature profile in Figure 10: (1) at the end of mechanical loads (50°F), (2) at the peak temperature 310°F, and (3) at the end condition of 80°F.

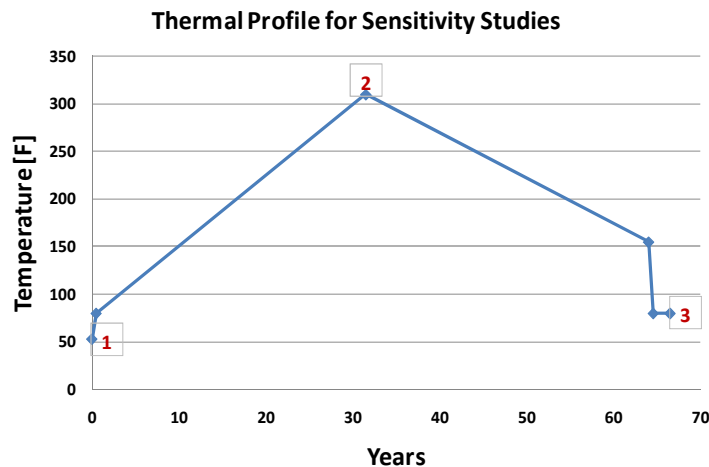


Fig 10. Thermal Profile Used in the Sensitivity Studies

Figure 11 shows the tank sections at which the forces and moments are evaluated for ACI demands and capacity calculations. As shown in this figure, the tank from the center of the dome to the center of the slab is divided into 42 sections for the force and moment evaluations. At each section the meridional force, hoop force, meridional moment, hoop moment and through wall shear demands are obtained from the ANSYS® finite element model results and are compared against corresponding section capacities calculated based on ACI 349-06 code provisions. The section numbers on the X-axis of all the results presented in Figures 13, 14, 16 and 17 correspond to the sections shown in Figure 11.

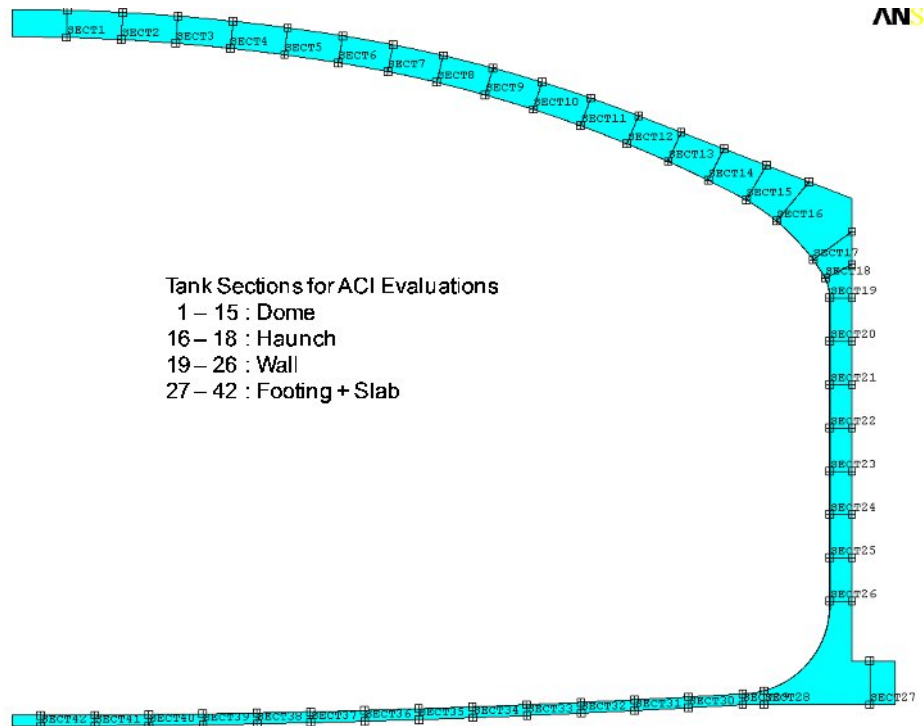


Fig 11. Tank Sections for Force and Moment Evaluations. Sections are numbered beginning at the center of the dome and progress around the tank profile to the center of the floor.

The results from sensitivity studies are presented as unfactored force and moment demand plots as well as unfactored ACI Demand/Capacity ratio plots. The force and moment demand plots alone were not sufficient to completely understand the net effect of force and moment variations. This is because the concrete section capacities are calculated based on the combination of section force and moment, which can vary considerably, especially if the section force changes from compression to tension. Therefore, the change in force and moment demand does not have an intuitive effect on the ACI Demand/Capacity ratios. The ACI Demand/Capacity comparison plots present the combined effect of the forces and the moments at any section. Of particular interest is the net effect of force and moment changes on the demands in the critical regions of the tank such as the haunch (sections 16–18), the top of the wall near the haunch (section 19), and the knuckle (section 28).

Soil Backfill Study

Figure 12 illustrates the details of the finite element model used for backfill sensitivity study. The model is very similar to the baseline model except that the excavation boundary is removed and the undisturbed soil surrounding the tanks is replaced with the backfill soil throughout the radial extent of the soil. The boundary conditions used in this model are the same as those in the baseline structural and thermal models described previously.

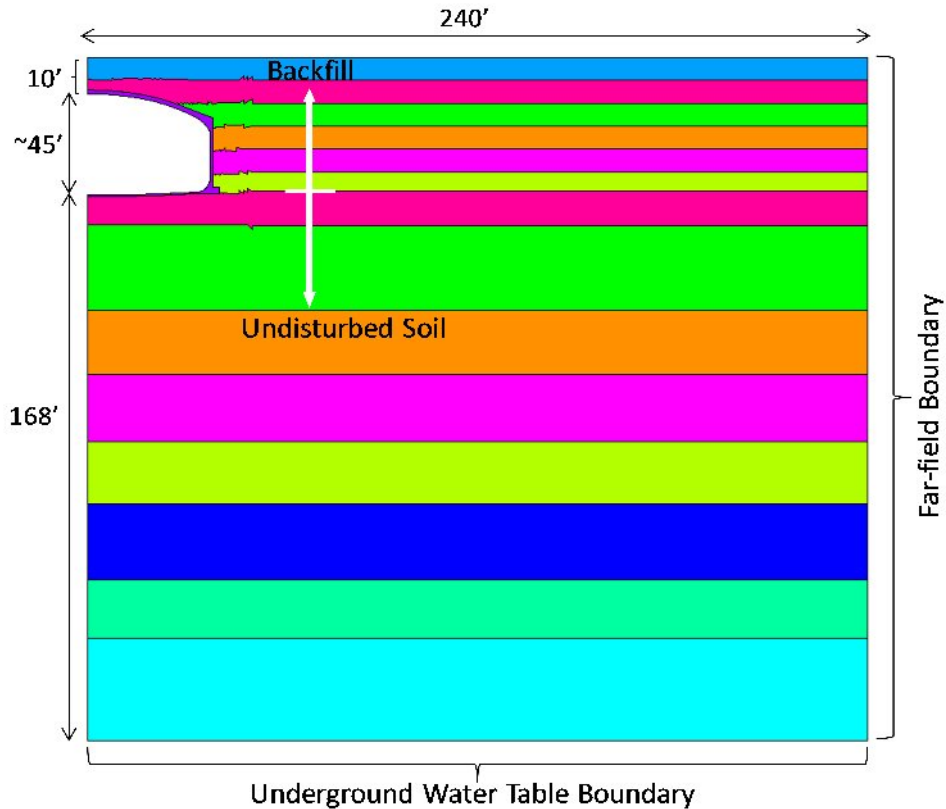


Fig 12. Details of the finite element Model for Backfill Study

Figures 13 (a) through (d) compare section demands for meridional force, meridional moment, hoop force, and hoop moment respectively, between baseline and backfill models. In these plots, the legend entries starting with “Base” and “BkFI” represent the results with the baseline model and backfill study model, respectively. The section numbers and the locations at which the force and moment demands are extracted were previously shown in Figure 11 and are the same for all the models.

The results from the backfill analysis model presented as force and moment plots in Figure 13(a) through (d) show that the main differences between baseline and backfill models appear in the circumferential demands in the haunch region, especially at the peak temperature 310°F and at the end condition of 80°F. This is evident from the hoop force (Fig 13c) and the hoop moment (Fig 13d) plots. From Figures 13(c) and 13(d) it is evident that the models with complete backfill (throughout the radial extent of the soil) produced higher circumferential demands (green lines) in the haunch region, especially at the peak temperature of 310°F. The hoop force plot shows increased tensile demand in the haunch sections 15 through 18, whereas the hoop moment plot shows increased demands at various sections in the dome and haunch. No significant differences in the demands are observed at other sections of the tank.

The net effect of these changes in circumferential force and moment demands in the dome and haunch is captured in the ACI Demand/Capacity comparison plots shown in Figure 14(a) through (c). The ACI Demand/Capacity ratio comparison for mechanical loads doesn't show any differences between the baseline and backfill models, however, the differences especially in the haunch region are considerable in the plots at the peak temperature of 310°F (Fig 14b) and also at the end temperature of 80°F (Fig 14c). Also the model with complete backfill showed

higher contact pressures at the soil concrete interface in the dome near haunch at the three evaluation points. These results from the backfill sensitivity study indicate that the model with backfill replacing the native soil predicts higher Demand/Capacity ratios and is conservative under ACI evaluations.

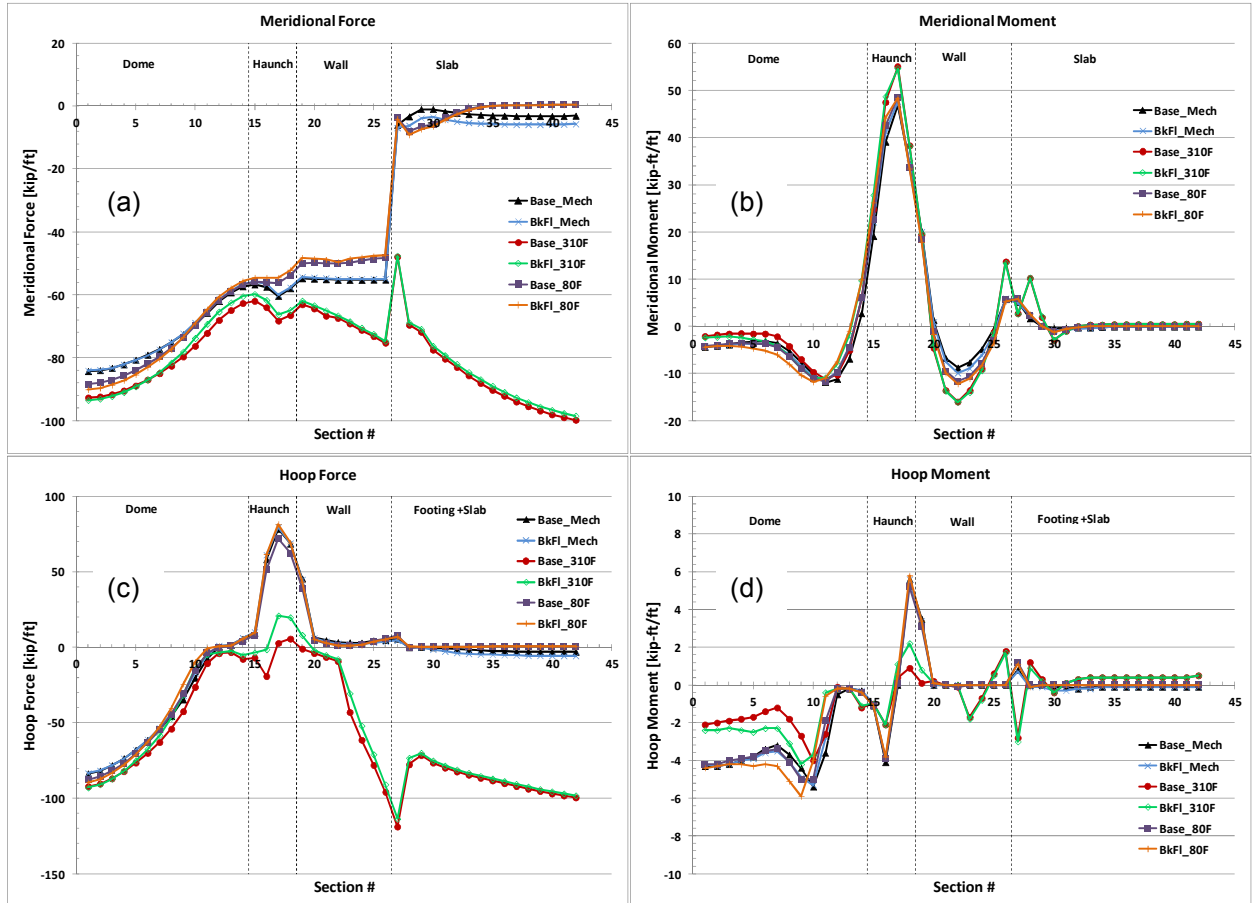


Fig 13. Baseline vs. Backfill Soil Demands Comparison (a) Meridional Forces (b) Meridional Moments (c) Hoop Forces (d) Hoop Moments

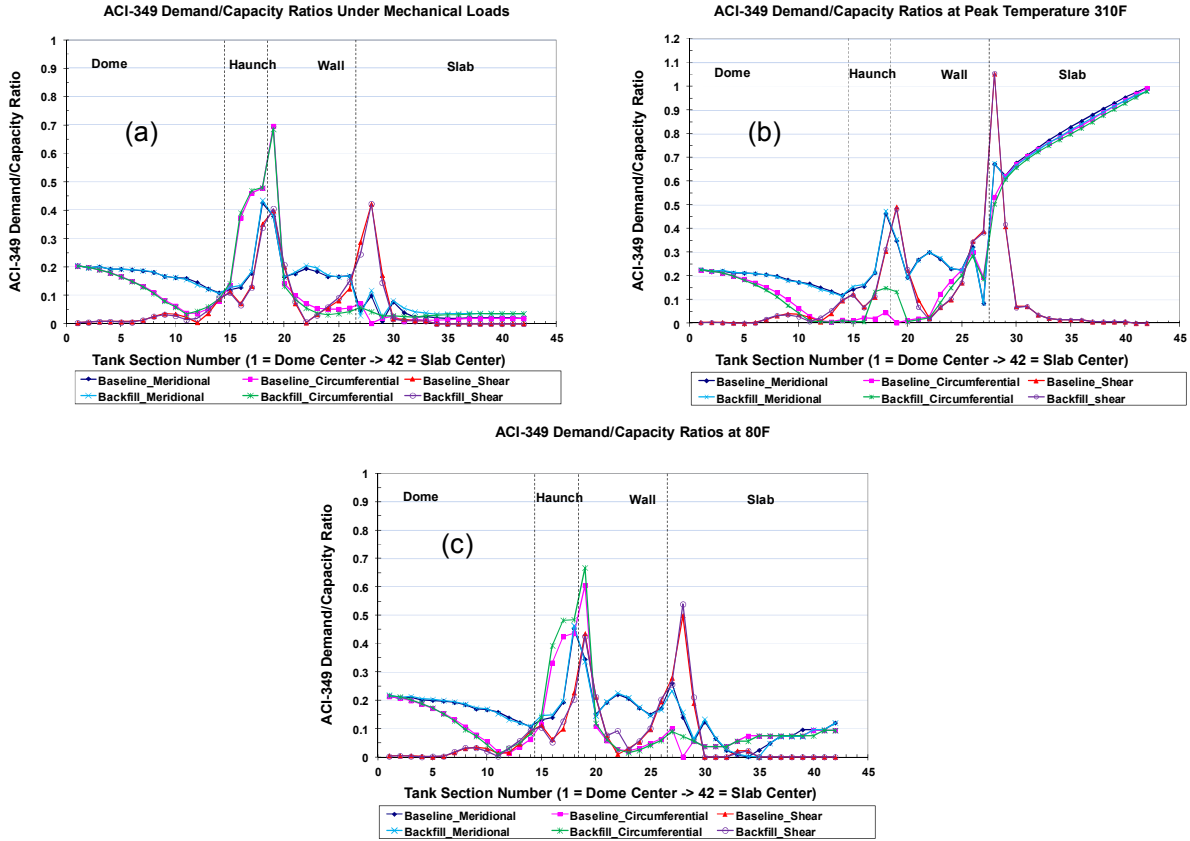


Fig 14. Baseline vs. Backfill Demand/Capacity Ratio Comparison (a) under Mechanical Loads (b) at Peak Temperature 310°F (c) at End Condition of 80°F

Soil Radial Extent Study

Sensitivity studies with the far-field soil dimension of 62 ft were carried out to investigate the effect of surrounding tanks by considering a fixed boundary at a distance of 62 ft from the tank (which is the distance to the adjoining tank) instead of 240 ft used in the baseline model. Figure 15 illustrates the details of the finite element model used for soil radial extent studies. Since the excavation boundary just starts at a distance of 10 ft from the outer radius of foundation slab (footing), no excavation boundary is included in these models.

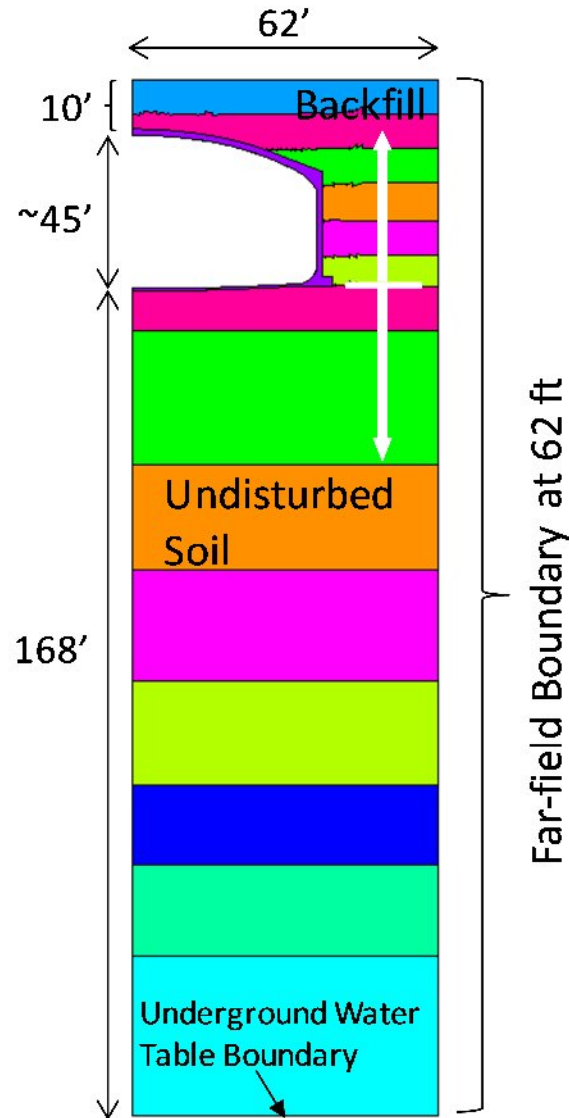


Fig 15. Details of the Finite Element Model for 62-ft Soil Radial Extent Study

The force and moment plots for this study [Figure 16(a) through (d)] show that the differences between the baseline and 62-ft radial extent models appear in the meridional force, circumferential force, and hoop moment demands at various sections in the tank, especially at the peak temperature 310°F and also at the end condition of 80°F. This is evident in the meridional force (Figure 16a), hoop force (Figure 16c), and hoop moment (Figure 16d) plots. In these plots, the legend items starting with “Base” and “Rx62” represent the results from the baseline model and the 62-ft soil extent model respectively. These plots show increase in the compressive demands at various sections in the tank at 310°F and 80°F. From the results showing comparisons of force and moment demands, it may appear that the model with 62-ft radial extent is conservative as it shows higher demands. However, that is not the case when these forces and moments are evaluated as ACI demands and capacities. Figures 17(a) through (c) compare the unfactored ACI demand/capacity ratios between the baseline and 62-ft radial extent models.

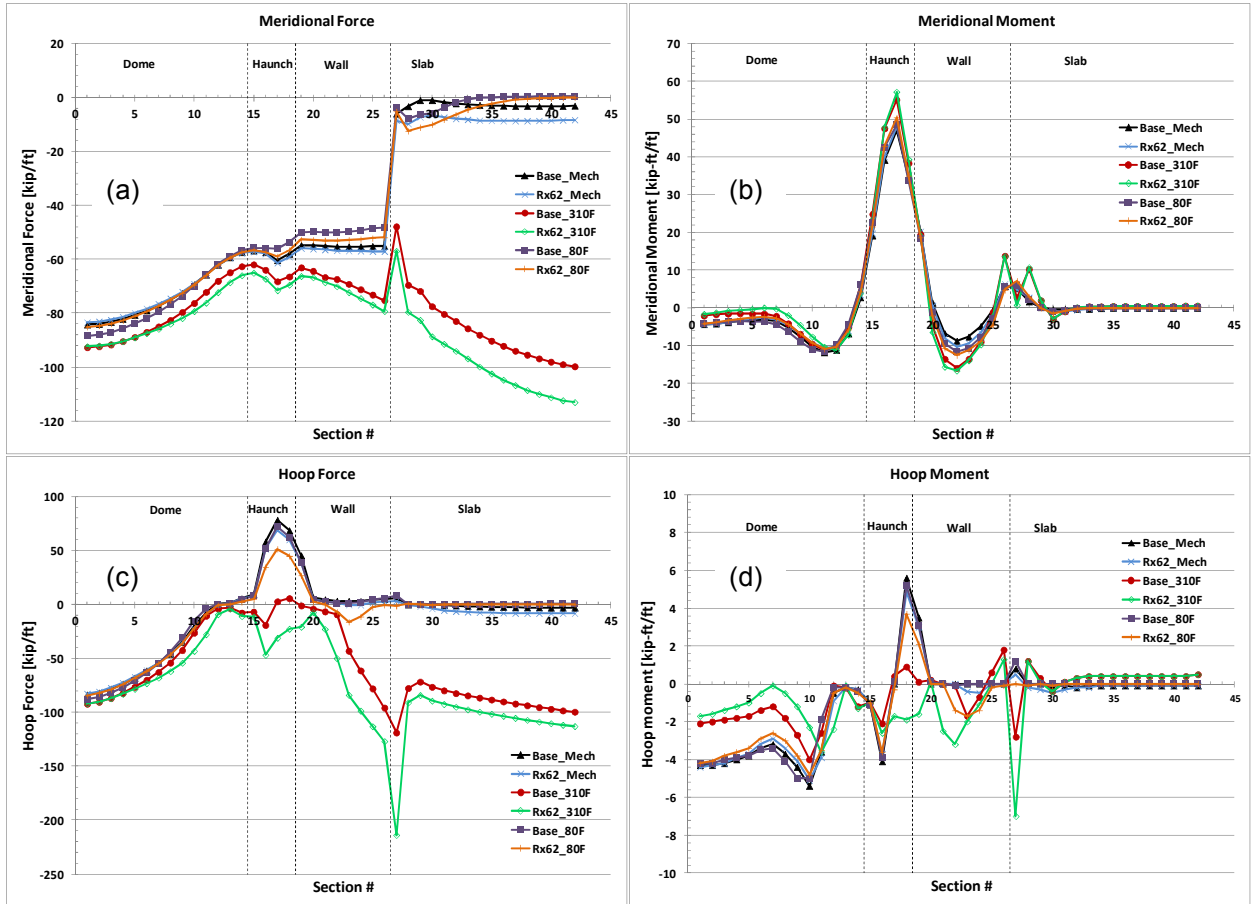


Fig 16. Comparison of Baseline vs. 62-ft Radial Extent Demands (a) Meridional Forces (b) Meridional Moments

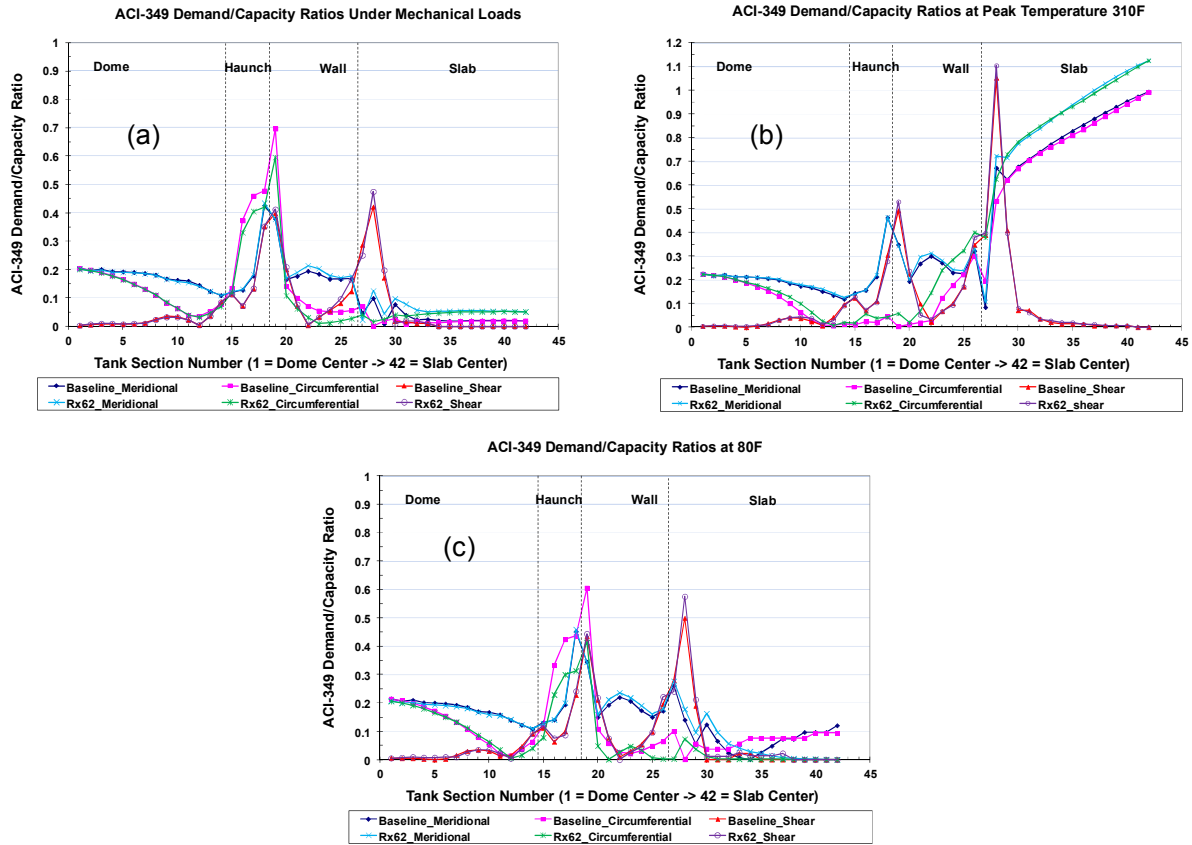


Fig 17. Comparison of Baseline vs. Backfill Demand/Capacity Ratios (a) under Mechanical Loads (b) at Peak Temperature 310°F (c) at End Condition 80°F

In general, the force and moment demand plots indicate that there are no significant differences in the meridional and shear demands (not shown) between the two models. The smaller radial extent (62 ft) case indicated slightly higher hoop (Fig 16c) compressive demands at the peak temperature (310F). However, the effect of this increase in compressive demands is very small when these results are evaluated as ACI Demand/Capacity ratios as shown in Figure 17(b). At the end condition of 80F, the baseline case produced slightly higher hoop force and moment demands especially near haunch region as shown in the Figure 16(c) and Figure 16(d) respectively. This resulted in increased hoop Demand/Capacity ratios in this section as shown in the Figure 17(c). For the purpose of ACI evaluations, the results that include conservatism at the end conditions are significant. The comparison of ACI Demand/Capacity ratios at the average Type-II tanks current conditions of 80°F (Fig 17c) indicate negligible differences in the meridional and shear ratios and clearly shows higher circumferential Demand/Capacity ratios in the baseline case.

The soil extent study shows that the baseline case with 240-ft radial soil extent gives conservative results under ACI evaluations. Furthermore, the model with backfill soil properties extending to the 240 ft boundary gives higher Demand/Capacity ratios that when the native soil properties are included in the outer region. Hence, the model with 240-ft radial soil extent and backfill properties throughout the radial extent was recommended and used in the analysis of record for single-shell tanks.

Conclusions

This article presented the details of the finite element models and analysis approach followed during the ongoing effort to establish structural integrity of single shell tanks at the Hanford site. The details of the material constitutive models applicable to the underground Hanford concrete tanks that capture the thermal and creep induced degradation are also presented. The thermal profiles were developed based on the available tank temperature data for the Type II and Type III single-shell tanks, and they were chosen to yield conservative demands under the thermal and operating loads analysis of these tanks. Sensitivity studies were conducted to address two issues regarding the soils modeled around the single-shell tanks. The results indicate that excluding the boundary separating the backfill soil from the undisturbed soil will result in conservative demands (plots 14b and 14c green lines for circumferential Demand/Capacity ratios). The radial extent study indicated that the soil model extending to 240 ft gave more conservative results than the model with 62 ft of soil (plots 17a and 17c magenta lines for hoop Demand/Capacity ratios). Based on these results, a 240 ft far-field soil boundary with backfill throughout the lateral extent was recommended and used for the finite element models used in the Type-II and Type-III analyses of record. The modeling effort and sensitivity studies discussed in this article helped in developing bounding models for the structural integrity evaluation of single shell tanks at the Hanford site.

Acknowledgement

The authors would like to acknowledge the management support of Washington River Protection Solutions and the funding they provided on behalf of the U.S. Department of Energy's (DOE's) Office of River Protection (ORP) to perform the Single Shell Tank Analysis of Record Project.

References

1. Johnson, KI, JE Deibler, FG Abatt, and MW Rinker. 2010. *Single-Shell Tank Structural Evaluation Criteria*. RPP-46442, Rev.0, Pacific Northwest National Laboratory, Richland, Washington.
2. ACI. 2007. *American Concrete Institute Code Requirements for Nuclear Safety Related Concrete Structures*. ACI 349-06, American Concrete Institute, Farmington Hills, Michigan.
3. Abatt GF, Stoops K, *Seismic Analysis Model Development for Hanford Single-Shell Structural Integrity*, WM2012 Conference, Phoenix, Arizona
4. Pilli SP, Rinker MW, *Structural Analysis Results of Thermal, Operating, and Seismic analysis for Hanford Single-Shell Tank Integrity*, WM2012 Conference, Phoenix, Arizona
5. Rinker MW, JE Deibler, KI Johnson, SP Pilli, CE Guzman-Leong, and OD Mullen. 2004. *Hanford Double-Shell Tank Thermal and Seismic Project – Thermal and Operating Load Analysis*.
6. Bander TJ, JP Day, AD Dyrness, RJ James, LJ Julyk, RS Marlow, CJ Moore, EW Pianka, YR Rashid, JS Shulman, and MP Weis. 1994. *Tank 241-C-106 Structural Integrity Evaluation for In situ Conditions*. WHC-SD-W320-ANAL-001, Revision 0, Volumes I and II, Westinghouse Hanford Company, Richland, Washington.
7. ANSYS®. 2011. ANSYS® Mechanical, Release 12. ANSYS Inc., Canonsburg, Pennsylvania.

8. Rinker MW, KI Johnson, SK Bapanapalli, NK Karri, JE Deibler, SP Pilli, CE Guzman-Leong, SE Sanborn, FG Abatt, JA Dewberry, BM Larsen, KL Stoops, and LJ Julyk. 2011a. “*Single-Shell Tank Integrity Project Analysis of Record: Hanford Type II Single-Shell Tank Thermal and Operating Loads and Seismic Analysis*” RPP-RPT-49989, Rev. 0, PNNL-20424, Pacific Northwest National Laboratory, Richland, Washington.
9. Rinker MW, KI Johnson, SK Bapanapalli, NK Karri, JE Deibler, SP Pilli, CE Guzman-Leong, SE Sanborn, FG Abatt, JA Dewberry, BM Larsen, KL Stoops, and LJ Julyk. 2011b. “*Single-Shell Tank Integrity Project Analysis of Record: Hanford Type III Single-Shell Tank Thermal and Operating Loads and Seismic Analysis*” RPP-RPT-49990, Rev. 0, PNNL-20739, Pacific Northwest National Laboratory, Richland, Washington.
10. Bazant ZP, O Buyukozturk, L Cedolin, TV Chang, WF Chen, K Gerstle, AR Ingraffea, J Isenberg, C Meyer, S Mirza, AA Mufti, D Murray, D Pecknold, WC Schnobrich, AC Scordelis, KJ William, TC Liu, D Darwin, and AH Nilson. 1982. *State-of-the-Art Report on Finite Element Analysis of Reinforced Concrete*. Prepared by the task committee on finite element analysis of reinforced concrete structures of the structural division committee on concrete and masonry structures, ASCE-1982.
11. Meyer C, and K Bathe. 1982. *Nonlinear Analysis of R/C Structures in Practice*. Journal of the Structural Division, Proceedings of the American Society of Civil Engineers, Volume 108, No. ST7, July 1982; Article 17216, pp. 1605–1622.